Environmental Pollution 258 (2020) 113712

Contents lists available at ScienceDirect

Environmental Pollution

journal homepage: www.elsevier.com/locate/envpol

Profiling epigenetic changes in human cell line induced by atrazine exposure☆

Oscar F. Sánchez [a, d], Li Lin [a], Chris J. Bryan [b], Junkai Xie [a], Jennifer L. Freeman [c], Chongli Yuan [a, *]

[a] Davidson School of Chemical Engineering, Purdue University, West Lafayette, IN, 47907, USA
[b] Department of Statistics, Purdue University, West Lafayette, IN, 47907, USA
[c] School of Health Sciences, Purdue University, West Lafayette, IN, 47907, USA
[d] Department of Nutrition and Biochemistry, Pontificia Universidad Javeriana, Bogotá, 110231, Colombia

ARTICLE INFO

Article history:
Received 3 October 2019
Received in revised form
12 November 2019
Accepted 30 November 2019
Available online 13 December 2019

Keywords:
Herbicide
Atrazine
Endocrine disrupting chemical
Epigenetics

ABSTRACT

How environmental chemicals can affect and exert their toxic effect at a molecular level has gained significant interest in recent years, not only for understanding their immediate health implications over exposed individuals, but also for their subsequent progeny. Atrazine (ATZ) is a commonly used herbicide in the U.S. and a long-suspected endocrine disrupting chemical. The molecular mechanism conferring long-term adverse health outcomes, however, remain elusive. Here, we explored changes in epigenetic marks that arise after exposure to ATZ at selected doses using image-based analysis coupled with data clustering. Significant decreases in methylated CpG (^{me}CpG) and histone 3 lysine 9 tri-methylated (H3K9me3) were observed in the selected human cell line with a clear spatial preference. Treating cells with ATZ leads to the loss of a subpopulation of cells with high ^{me}CpG levels as identified in our clustering and histogram analysis. A similar trend was observed in H3K9me3 potentially attributing to the cross-talking between ^{me}CpG and H3K9me3. Changes in ^{me}CpG are likely to be associated with alterations in epigenetic enzyme expression levels regulating ^{me}CpG and persist after the removal of ATZ source which collectively provide a plausible mechanism for long-term ATZ-induced toxicity.

1. Introduction

Exposure to environmental stressors such as air pollutants and environmental chemicals have long been associated with various adverse health outcomes, such as different types of cancers, central nervous system disorders (e.g., Parkinson's disease) and reproductive dysfunctions (e.g., decreased fertility in both males and females and increased chance of miscarriage)(Mark et al., 2012; Mostafalou and Abdollahi, 2013). Recent literature evidence suggests that the health implications of some environmental chemicals no only affect exposed individuals but also their subsequent progeny(Skinner et al., 2010; Hanson and Skinner, 2016). Endocrine disrupting chemicals (EDCs), are one of those environmental chemicals. EDCs are primarily known to disrupt endogenous hormone signaling pathways (Uzumcu et al., 2012; Alavian-Ghavanini and Rüegg, 2018). They have diverse chemical structures and can be found in numerous consumer products including plasticizers, pharmaceuticals, and pesticides, making human exposure a likely event(Uzumcu et al., 2012). EDCs are known to increase the risk of various chronic diseases and conditions, i.e., neurodegenerative diseases and reproductive functions(Schug et al., 2011). The chronic effects of EDC have been attributed to alterations in epigenome that arise immediately after exposure but can be persistent over lifetime (Xin et al., 2015; Tapia-Orozco et al., 2017; Alavian-Ghavanini and Rüegg, 2018) and potentially inherited across generations(Diamanti-Kandarakis et al., 2009).

Atrazine (ATZ, 2-chloro-4-ethylamino-6-isopropylamino-1,3,5-triazine) is a globally used herbicide and its usage peaks in the Midwestern regions of the United States. The estimated use of ATZ is ~76 million pounds per year(Kiely et al., 2004; Thelin and Stone, 2010). ATZ has low biodegradability, high solubility (30 mg L^{-1} at 20 °C) and is commonly found in ground and surface water (Graymore et al., 2001) rendering easy access for animal and human consumptions. ATZ has long been suspected to be an EDC.

☆ This paper has been recommended for acceptance by Wen Chen.
* Corresponding author.
E-mail address: cyuan@purdue.edu (C. Yuan).

https://doi.org/10.1016/j.envpol.2019.113712
0269-7491/

Damages to reproductive organs, liver and kidney have been reported due to excessive ATZ ingestion using different animal models (Nightingale et al., 2007; Xing et al., 2012; Wang et al., 2013; Liu et al., 2014; Wirbisky and Freeman, 2015; Sena, 2017). Excessive exposure to ATZ has also been found to be associated with increased risks in Parkinson's disease and non-Hodgkin's lymphoma (Pathak and Dikshit, 2011; Sun et al., 2017;Wirbisky and Freeman, 2015) Understanding the molecular origin of these sustained damages induced by ATZ, epigenetic alterations in particular, is thus of pressing need to address the potential health risk arising from this emerging environmental chemical.

Epigenome consists of posttranslational modifications (PTMs) of histones, i.e., methylation and acetylation of histone H3 and H4, and non-genetic modifications of nucleic acids, i.e., methylation of cytosines in a CpG content (^{me}CpG). Collectively, they create epigenetic landmarks that dictate the transcriptional state of cells. Few studies exist accounting for ATZ effects on epigenome. Recently, studies from our own group and others' have revealed that ATZ can alter DNA methylation by affecting the enzymatic activity of DNA methyltransferase particularly DNA methyltransferase 1 (DNMT1) (Wang et al., 2014; Xing et al., 2015; Wirbisky-Hershberger et al., 2017). ATZ was also found to cause downregulation of trimethylation to the lysine 4 on the histone H3 protein (H3K4me3) in a mice model(Hao et al., 2016). The epigenetic effects of ATZ on human cells, however, remain elusive.

To address the current knowledge gap, we utilized *in situ* probes developed in our laboratory (Sanchez et al., 2017) and expanded their capability to track various types of epigenetic modifications in human kidney cells lines (HEK293T). This cell line was selected as a model system, since extensive evidence exists suggesting that ATZ gets enriched and degraded in human kidneys (Perry et al., 2000; Catenacci et al., 2002; Lebov et al., 2016), thus making it an organ susceptible for ATZ induced damages. Our results suggest that ATZ can induce significant changes in ^{me}CpG and H3K9me3, both of which are known to persist over time and are critical for the formation of heterochromatin containing repressed genes. The changes as observed seem to be dose-dependent with larger doses affiliated with more significant alterations. A machine-learning based clustering and variable selection approach was used to identify cells with distinctive epigenetic features and identified intensity-related features as the most distinctive in clustering ATZ treated and untreated cell sub-populations. Compared to histone methylation, ^{me}CpG was found to be a better classifier of ATZ treated cells and was tracked *in situ*. ATZ induced ^{me}CpG changes were found to persist after the removal of ATZ source.

2. Materials and methods

2.1. Protein sensors for monitoring epigenetic marks

In situ epigenetic probes were developed as we reported in our previous publications (Kim et al., 2014; Sanchez et al., 2015). For improved signal quality, we utilized a bimolecular fluorescence complementation (BiFC) strategy as shown in Fig. S1A (Supporting **Information**). All probes share modular designs including a "recognition" motif and a fluorescent domain (see Fig. S1B **(**Supporting **Information))**. The sequence of the "recognition" motifs for ^{me}CpG and H3K9me3 are derived from known epigenetic "reader" domains that have been verified either in our own work (Kim et al., 2014; Sanchez et al., 2015; Sanchez et al., 2017) or previous literature (Fischle et al., 2008). Typical images of HEK293T cells transfected with our engineered probes are shown in Fig. S2 (Supporting **Information**). The fluorescent foci and islands as observed in these images reflect the spatial location of chromatin rich in the epigenetic modification of interest, while their intensity can be related to the abundance of selected epigenetic marks *in situ* (Capoulade et al., 2011; Gonzalez-Sandoval et al., 2015; Sanchez et al., 2017).

2.2. Mammalian cell culture and transfection

Human embryonic kidney 293T (HEK293T) cells were cultured as described previously(Sanchez et al., 2017). Briefly, cells were cultured in Dulbecco modified Eagle medium supplemented with 10% (v/v) fetal bovine serum and 1% (v/v) of a Penicillin-Streptomycin solution (Gibco®, CA, US), and incubated at 37 °C with 5% CO_2. Engineered sensors were transiently transfected into HEK293T conducted using Lipofectamine® 3000 (Life Technologies, MD, US) following the manufacture's protocol.

2.3. Chemical treatment of HEK293T cells

ATZ stock solutions were prepared as we described previously (Wirbisky and Freeman, 2015; Wirbisky-Hershberger et al., 2017) and spiked into cell culture media at selected concentrations. HEK293T cells were exposed to ATZ concentrations of 0, 3 and 30 parts per billion (ppb; μg/L) ppb. Images of transfected HEK293T cells were collected after 48 h of ATZ treatment. The ATZ concentrations were selected based on the known toxicity of ATZ and current Environmental Protection Agency (EPA) regulation standard (EPA, 2016; Mostafalou and Abdollahi, 2017) which are detailed later in the Results section.

Atrazine toxicity over exposed HEK293T cells was evaluated by monitoring different parameters such as cell metabolic activity, cell growth, presence of double-strand breaks (DSBs) in the DNA, and nuclear size and eccentricity. Cell metabolic activity was assessed using a commercial MTT kit (Abcam, U.S) according to manufacturer's recommendations. HEK293T growth was monitored under different ATZ concentrations via the live/dead assay using Trypan blue. To detect if exposure to ATZ causes cytotoxic lesions in the genome of HEK293T cells, we stained for double strand breaks in DNA via γH2A.X staining (Invitrogen, U.S.).

2.4. Fluorescent microscopy

Transfected cells were imaged using a Nikon Eclipse Ti-2 inverted microscope using 60 × /1.49 NA oil objective as we described previously (Sanchez et al., 2017). Z-stack images of cells were collected using Nikon EZ-C1 software with 0.80 μm interval. 2D projections of collected Z-stack images were analyzed using CellProfiler (Broad Institute (Carpenter et al., 2006)) to get the Integrated Intensity per Nuclei (IIN). This parameter was used to quantify epigenetic modification level per cell as have been demonstrated in our previous work (Sanchez et al., 2017; Sánchez et al., 2019) and others (Hayashi-Takanaka et al., 2011; Lungu et al., 2017).

2.5. Quantitative polymerase chain reaction (qPCR)

HEK293T cells were treated with ATZ and total RNA was extracted using an RNA purification kit (PureLink, Thermo Fisher Scientific, U.S.) following the manufacturer's protocol. cDNA was prepared using SuperScript IV Reverse Transcriptase (Thermo Fisher Scientific, U.S.) and random hexamers. qPCR was carried out using QuantStudio 3 (Thermo Fisher Scientific, U.S.) with a standard cycling condition. PowerUp SYBR Green (Thermo Fisher Scientific, U.S) was used in the reaction mixture. Primers used to measure the expression level of selected epigenetic "writers" and "erasers" are summarized in Table S1 (Supporting **Information**). β-Actin (ACTB) was used as the reference gene. qPCR was performed in accordance

with the MIQE requirements (Bustin et al., 2009).

2.6. Flow cytometry

Flow cytometric data were collected using a BD FACS Aria Cell Sorter (Becton Dickson, San Jose, CA). A 488 nm excitation laser line and a 530/30 nm FITC filter was used for capturing GFP fluorescence intensity. All cytometry data was analyzed using FCS Express software (De Novo software, Glendale, CA).

2.7. Statistical analysis

All statistical analysis and error propagation calculations were performed in OriginPro 2018 (Origin Lab Corp, North Hampton, MA) statistical software. An analysis of variance (ANOVA) followed by a Tukey's HSD post-hoc test was used when a significant ANOVA was observed ($\alpha < 0.05$). Origin Pro and Graphpad Prism were used for analysis. Principle Component Analysis (PCA) and clustering analysis was performed using R-studio.

3. Results

3.1. Low dose of ATZ does not elicit immediate phenotypic changes in the human cell line HEK293T

We started by examining the toxicity of selected ATZ concentrations on HEK293T cells. Fig. 1A summarized our findings using the MTT assay. No significant changes were observed at the selected ATZ doses, suggesting no significant alterations in cell metabolic activities. Fig. 1B examined the growth curves of HEK293T treated with ATZ. Increasing ATZ concentrations seem to slightly slow down cell growth, but the changes were found not to be statistically significant. We then stained exposed HEK293T cells with γH2A.X antibody, which gets enriched in DNA with DSBs and thus represents the chance of exposed cells to acquire DNA mutations. Our results (Fig. 1C) indicated that no γH2A.X foci can be observed after treating cells with the selected doses of ATZ. ATZ at 3 or 30 ppb is thus not a potent mutagen for HEK293T cells. We further analyzed the nuclear size and eccentricity of exposed cells and the results are summarized in Fig. 1D. Exposure to ATZ does not significantly alter the nuclear size or eccentricity.

3.2. Low dose ATZ affects H3K9me3 distribution and abundance

To assess how exposure to ATZ affects H3K9me3 distribution and abundance, we used our *in situ* H3K9me3 probes. Our probes are enriched in chromatin regions with high H3K9me3 contents, which can be recognized as bright spots within the cell nucleus and near cell periphery. Images of transfected cells under varying ATZ concentrations were summarized in Fig. 2A. Typical 2D slice images used to construct z-stacked images can be found in Fig. S2A (Supporting **Information**). Untreated cells exhibit bright H3K9me3 dots forming a rim at the nuclear periphery corresponding to perinuclear heterochromatin regions as previously reported in literature (Politz et al., 2013). Bright island-like features are also observed within cell nucleus corresponding to intra-nuclear chromatin regions rich in H3K9me3. After ATZ treatments, we observed that H3K9me3 islands and foci become significantly dimmer (see also Fig. 2A). The overall brightness of cells representing global H3K9me3 levels drops with increasing ATZ concentrations. Furthermore, the rim consisting of H3K9me3-rich islands near nuclear periphery gradually disappeared after treating cells with increased ATZ doses. To rule out the possibility that the observed changes could originate from different expression levels of transfected probes, control experiments were performed using cells transfected with a negative control consisting of a nuclear localization signal fused to EGFP (NLS − EGFP) with typical images shown in Fig. S3 (Supporting **Information**). No significant changes were observed among all treated groups, suggesting that ATZ treatment is not a significant factor in altering probe expression levels.

To quantify the observed changes, we characterized the intensity, morphology and texture features per cell accounting for the foci-like features formed by clustered H3K9me3 using CellProfiler. Typical images showing nuclei and H3K9me3 foci identified via our customized CellProfiler pipeline can be found in Fig. S4 (Supporting **Information**). These features were gathered and quantified for each cell which were then clustered using a PCA approach. PCA is a dimensionality reduction approach used in machine learning and data mining to identify a linear combination of parameters that can maximize the difference among treatment groups. Mean Gini index as shown in Fig. S5 (Supporting **Information**) illustrates the features with the largest weighted average of the Gini impurity criterion, a metric of variable importance, in a random forest model trained to classify between treated and untreated cells. To validate the selected features, adaptive LASSO (Least Absolute Shrinkage and Selection Operator) was also performed, which has been shown to provide consistent model selection in high-dimensional datasets(Wei et al., 2011). Although the exact features selected are not identical between the two methods, there was significant overlap. In addition, the categories of features selected (in terms of intensity, foci, texture, and morphology) were consistent among top features in both methods.

Among top selected features by both LASSO and Gini, intensity features near the nuclear periphery (edge) is found to be the most significantly different among treated groups which is consistent with our visual observations. All cells are mapped to the calculated principal component (PC) space as shown in Fig. 2B. We then performed unsupervised cluster analysis within the principal components using k-means clustering. As determined by the elbow plot (Fig. S6A, Supporting Information), the marginal gain in the percentage of variance explained was lowest at n = 3. We thus performed k-means clustering using 3 clusters. Untreated ATZ cells primarily fall within a single cluster. Cells treated with 3 and 30 ppb shows increased levels of dispersion in the PC space and form distinctive subpopulations, making up the majority of cluster 2 and 3 (see Fig. 2B). Among all measured features, we compared the Integrated Intensity per Nuclei (IIN) among treated groups (see Fig. 2C). IIN was found to correlate with global epigenetic modification level per cell as have been demonstrated previously by our group (Sanchez et al., 2017; Sánchez et al., 2019) and others (Hayashi-Takanaka et al., 2011; Lungu et al., 2017). Exposure to ATZ significantly lowers the global H3K9me3 levels, by 14% and 29% for ATZ concentrations of 3 and 30 ppb, respectively. Histograms illustrating inter-cellular heterogeneity in H3K9me3 levels are shown in Fig. 2D. The probability histograms show a positive skewed distribution shape which were individually fitted with a bimodal distribution (with R^2 = 0.93, 0.96 and 0.93 for 0, 3 and 30 ppb of ATZ, respectively). All fittings result in randomly distributed residuals suggesting good fitting quality. All treated groups feature two subpopulations of cells with distinctive H3K9me3 levels. ATZ treatments result in more cells with low H3K9me3 levels manifested as a significant broadening of the low-intensity subpopulation peak.

We further validated the changes in H3K9me3 distribution via FACS as shown in Fig. 2E. Compared to images analysis, FACS is advantageous in being able to analyze large number of cells in a short time, i.e., 10^4–10^5 compared to ~200 in image analysis. The result of FACS exhibits a similar bimodal distribution with a low- and high-fluorescent-intensity species, consistent with our

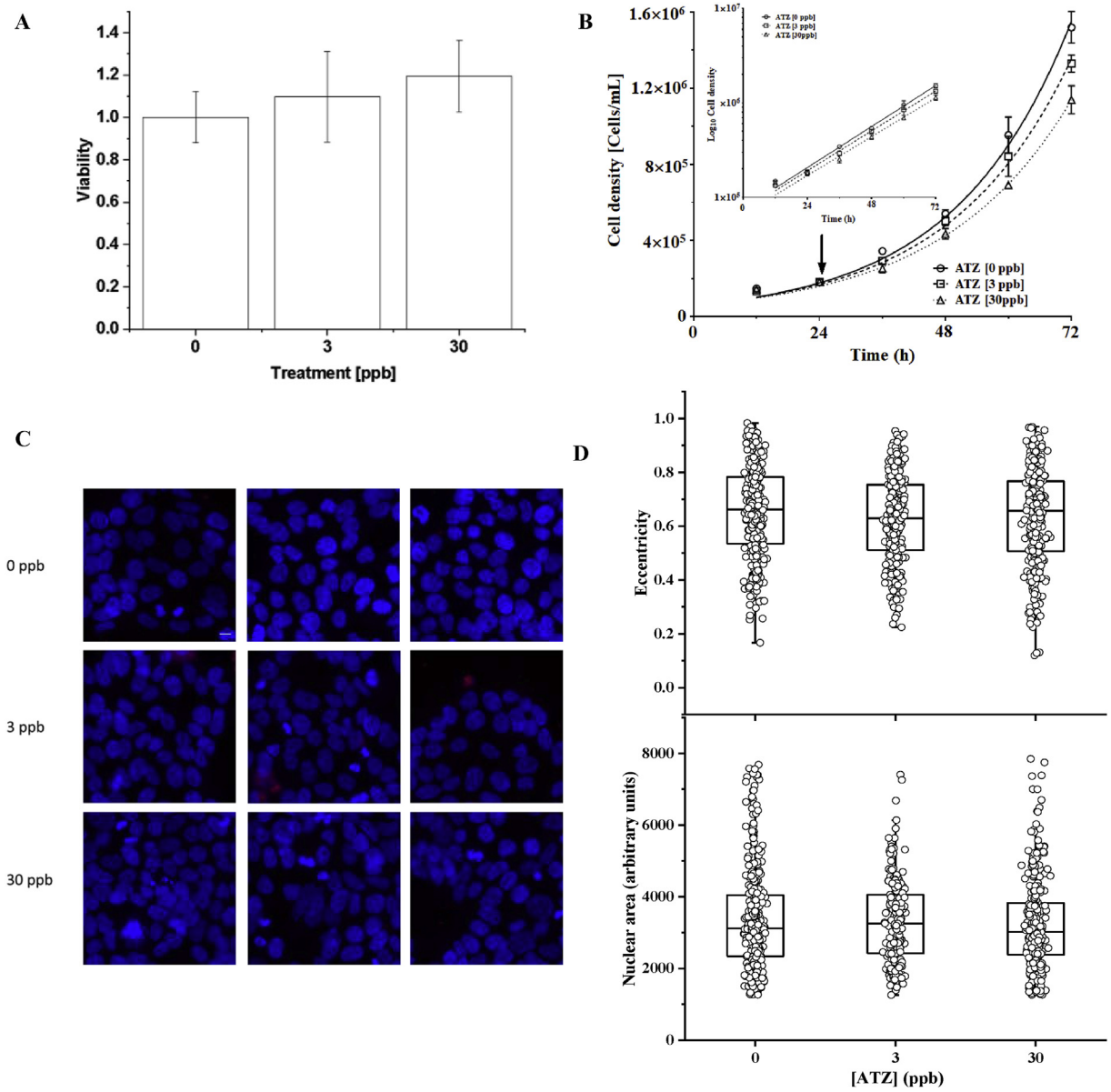

Fig. 1. No significant toxicity effects are induced by exposure to ATZ on HEK293T cells. A. Cell survival was assessed by MTT assay. The results represent the means of 3 independent experiments. No significant ($p > 0.05$) changes were observed at the selected ATZ doses, 3 and 30 ppb. **B.** Growth curves of HEK293T after treating with ATZ, 3 and 30 ppb. ATZ treatment slow down cell growth, but no significant ($p > 0.05$) effect was found in the doubling time (15.9 h, 16.8 h and 17.6 h for 0, 3 and 30 ppb of ATZ, respectively). **C.** Representative images of HEK293T cells treated with varying doses of ATZ and stained for γH2A.X (red). **D.** Exposure to ATZ revealed no significant ($p > 0.05$) modification in the nuclear size or eccentricity. (For interpretation of the references to colour in this figure legend, the reader is referred to the Web version of this article.)

microscopy-based image analysis. ATZ treatments significantly increased the abundance of cell subpopulations low in H3K9me3 levels. The drop in median intensity of ATZ treated samples were found to be ~15% and 28% for 3 and 30 ppb ATZ, respectively, which are in a close accordance with our image analysis (see also Fig. 2C). Collectively, this comparison suggests that our image analysis can capture the intrinsic heterogeneity in H3K9me3 levels with a similar accuracy to FACS analysis.

qPCR was then performed to reveal the potential molecular mechanism leading to the observed epigenetic changes. Specifically, we determined changes in transcriptional level of KMT1A and KDM4A as shown in Fig. 2F and Table S1 (Supporting **Information**). KMT1A and KDM4A are histone methyltransferase and demethylase that are highly specific for H3K9me3(Hyun et al., 2017). No statistical difference among the treatments was observed in the mRNA level of KMT1A or KDM4A.

3.3. Exposure to ATZ at low dose can result in ^{me}CpG changes in HEK293T cells

Representative images of HEK293T cells transfected with ^{me}CpG probes (*z*-projection) are shown in Fig. 3A. Fig. S2B (Supporting **Information**) depicts a representative set of 2D slice images used to get a z-projection. In untreated cells, we observed clustered ^{me}CpG islands as distinctive bright foci primarily located within cell nuclei. A few bright foci can also be found near the nucleus periphery, but they do not form a distinctive rim as we observed for H3K9me3 in the previous section. The observed methylation pattern is consistent with what has been previously reported in literature via immunostaining (Jørgensen et al., 2006; Barreto et al.,

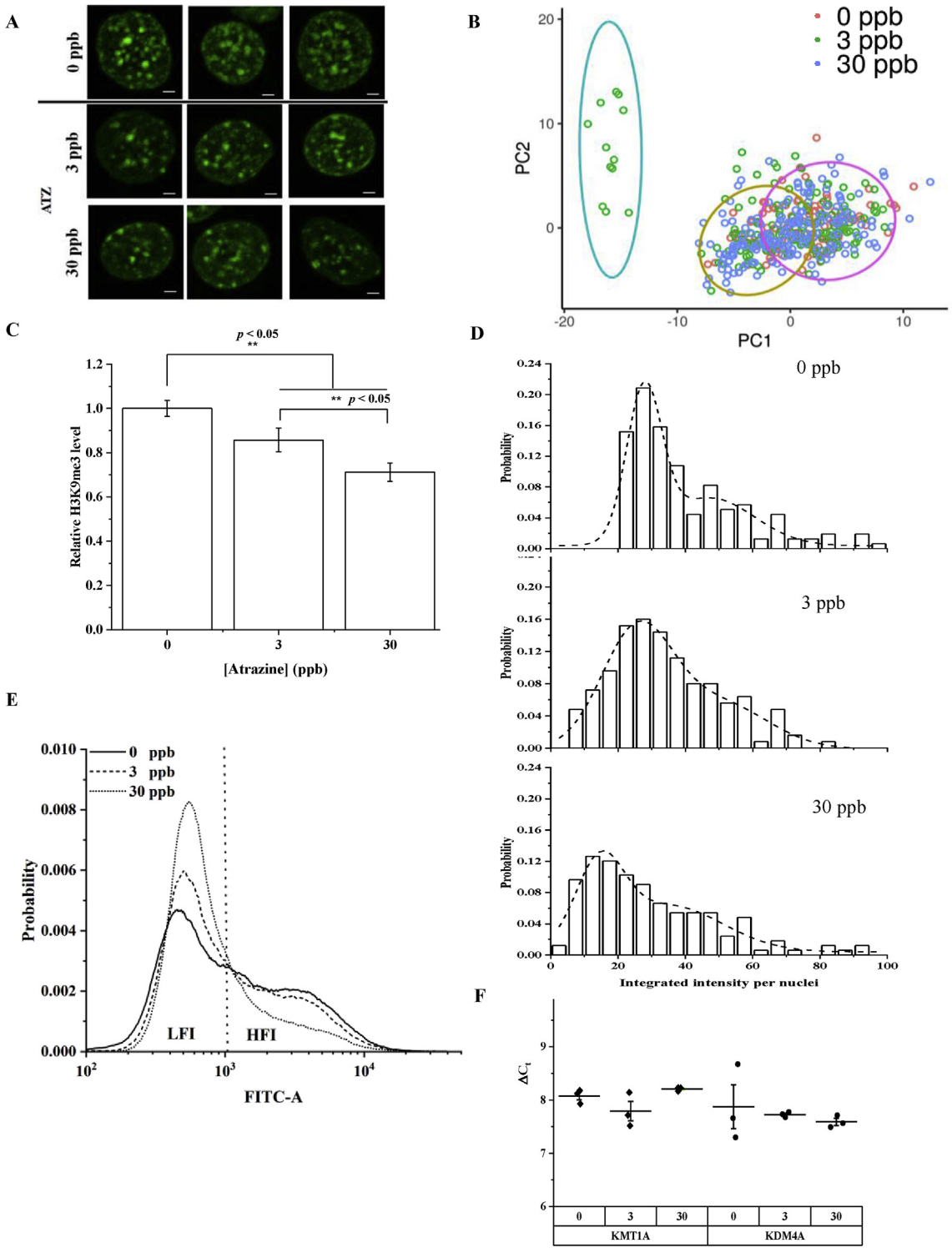

Fig. 2. H3K9me3 levels in HEK293T cells exposed to ATZ. A. 2D projected images of cells after 24 h of transfection with H3K9me3 sensors and pre-exposed for 24 h to ATZ at different concentrations. Scale bar = 2 μm. **B.** Principal component analysis of differentially expressed genes. Principal component 1 and 2 (PC1 and PC2, respectively) were selected as the axes explaining most of the data variance. **C.** Relative H3K9me3 levels to the control or 0 ppb of ATZ using the integrated intensity per nuclei obtained from image analysis. **D.** Probability density distribution of the integrated intensity per nuclei obtained from single cell image analysis, n ≥ 90, after ATZ treatment. **E.** FACS probability density distribution of the fluorescence intensity obtained from HEK293T cell populations treated at various ATZ concentrations (0, 3 and 30 ppb). **F.** Expression of mRNAs coding for KMT1A and KDM4A. Data are expressed as cycle threshold (Ct) difference to β-actin presented as dot plots with indicated mean value.

2007; Lungu et al., 2017). Exposure to ATZ leads to a significant loss of number of foci within cell nucleus and decrease in fluorescent intensity per cell. A PCA analysis was performed similar as described in the previous section with results shown in Fig. 3B and Fig. S5B (Supporting **Information).** Top ranked features based on both random forest clustering and LASSO analysis consisted

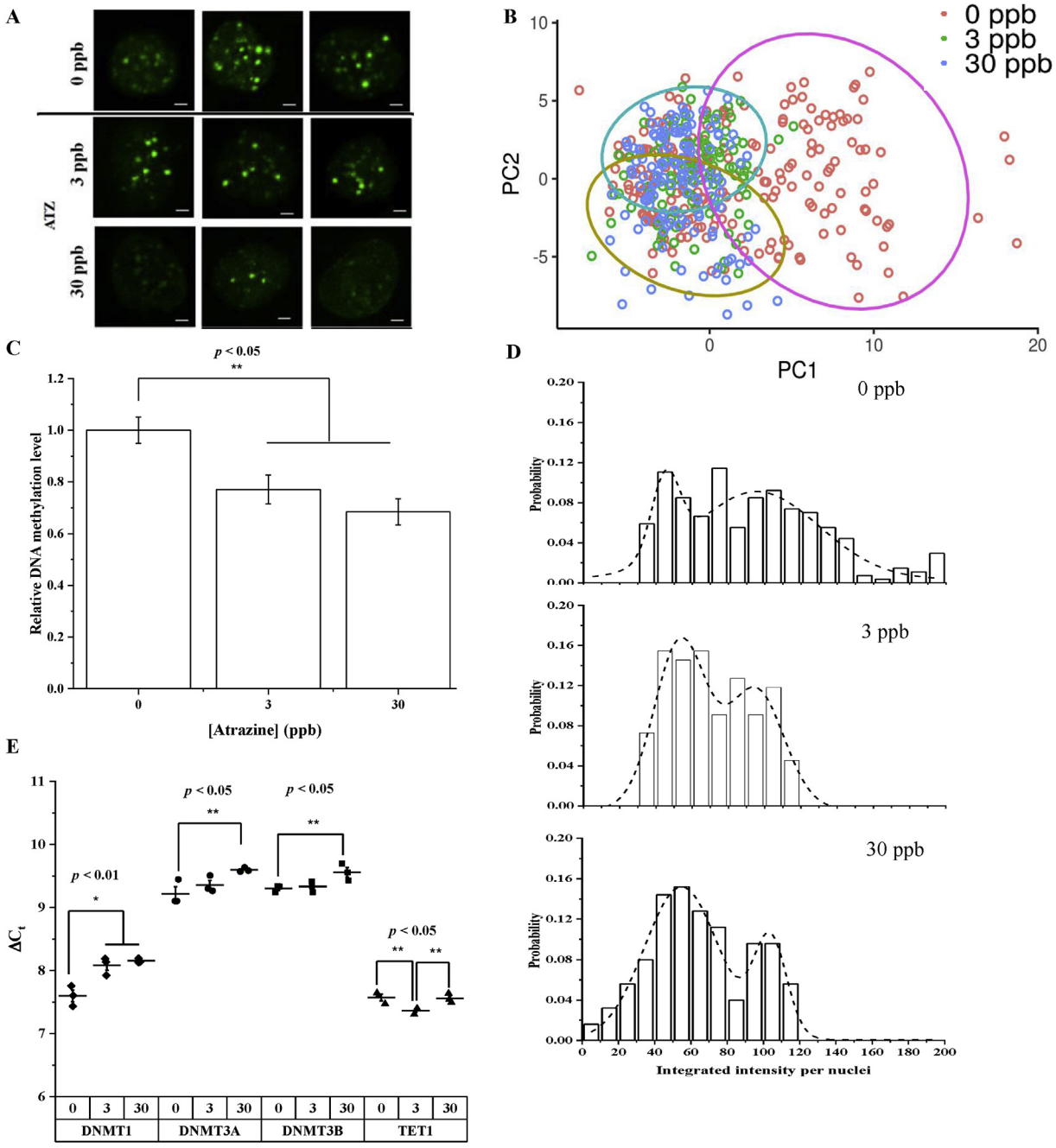

Fig. 3. DNA methylation levels in HEK293T cells exposed to ATZ. A. 2D projected images of cells after 24 h of transfection with ^{me}CpG-BiFC protein sensors and pre-exposed for 24 h to ATZ at different concentrations. Scale bar = 2 μm. **B.** Principal component analysis of differentially expressed genes. Principal component 1 and 2 (PC1 and PC2, respectively) were selected as the axes explaining most of the data variance. **C.** Relative DNA methylation levels to the control or 0 ppb of ATZ using the integrated intensity per nuclei obtained from image analysis. **D.** Probability density distribution of the integrated intensity per nuclei obtained from single cell image analysis, n ≥ 90, after ATZ treatment. **E.** Expression of mRNAs coding for DNMT1, DNMT3A, DNMT3B and TET1. Data are expressed as cycle threshold (Ct) difference to β-actin presented as dot plots with indicated mean value.

primarily of intensity-related variable, suggesting ATZ-treated groups have distinctive changes in ^{me}CpG intensities at different locations. Interestingly, although the difference of ^{me}CpG in the nuclear periphery region was not immediately obvious by visual inspections, the most distinctive feature among treated and untreated group was found to be the abundance of ^{me}CpG near the nuclear periphery, similar to what we have observed in H3K9me3. All collected cells were mapped to PC space as shown in Fig. 3B. Three clusters were identified using elbow plots as described in the previous section. Among these three clusters determined by unsupervised k-means, one cluster consists almost entirely of untreated cells, while other two clusters consist of a mixture of both untreated cells and cells exposed to two different doses of ATZ. These results suggest that a distinctive subpopulation characterizing of unique ^{me}CpG features seems to be disappearing after ATZ treatments.

We then proceeded to quantify changes in global ^{me}CpG levels per cell since our PCA analysis indicates that the integrated cell intensity is a good classifier for cells with and without ATZ treatment. Fig. 3C and D shows a bar plot and histograms comparing IIN

among different treatment groups. Consistent with our visual observation, ATZ treated cells show significant reductions in integrated cell intensity corresponding to decrease in ^{me}CpG methylation level. A drop of 23 and 32% in ^{me}CpG were observed for cells exposed to ATZ of 3 and 30 ppb, respectively. Fig. 3D visualize the intrinsic heterogeneity in ^{me}CpG among untreated and treated HEK293T cells. The probability histograms for the integrated intensity per cell are best fitted using a bimodal distribution (with $R^2 = 0.86$, 0.95 and 0.97 for 0, 3 and 30 ppb of ATZ, respectively). After ATZ treatments, the histogram shows a significant narrowing in distributions with loss of cells originally high in ^{me}CpG contents. The peak height and width of the low-^{me}CpG subpopulation also increased with increasing ATZ concentrations.

qPCR was then performed to shed light on the underlying molecular mechanism leading to the observed ^{me}CpG changes. We determined relative changes in DNA methyltransferase, namely DNMT1, DNMT3A and DNMT3B and methylcytosine dioxygenase, namely TET1. Fig. 3E and Table S2 **(**Supporting **Information)** summarize our qPCR findings. ATZ treatments significantly ($p < 0.01$) reduces the transcription level of DNMT1 (maintenance DNMT) with an average expression fold change of 0.72 and 0.68 at ATZ 3 and 30 ppb, respectively. mRNAs of *de novo* DNA methyltransferases 3A and 3B (DNMT3A and DNMT3B) were only significantly ($p < 0.05$) reduced at 30 ppb of ATZ, showing an expression fold change of 0.76 and 0.84, respectively. TET1 mRNA was significantly ($p < 0.05$) increased at 3 ppb of ATZ, with an expression fold change of 1.15. The observed changes can thus at least partially explain the drop in ^{me}CpG as we have observed in this study.

3.4. Persistency in the acquired ^{me}CpG changes

Epigenetic changes are potentially reversible due to the presence of epigenetic writer and eraser enzymes. For example, DNA methylation is established by *de novo* DNMTs (i.e., DNMT3A and 3B) and maintained by DNMT1; and the removal of DNA methylation can be facilitated by TET enzyme families (Bird, 2002). The altered DNA methylation profiles can be potentially recovered by the intrinsic epigenome repairing systems (Flatau et al., 1984). We thus proceeded to evaluate the persistency of acquired epigenetic changes. Between H3K9me3 and ^{me}CpG, ^{me}CpG was found to be a better characteristic for differentiating among treated and untreated cells because of higher average silhouette width and classification accuracy using a random forest model trained using intensity-based features (Fig. S7C (Supporting **Information**)). We thus proceeded to evaluate the short-term persistence of the acquired ^{me}CpG changes.

HEK293T cells transfected with ^{me}CpG probes were tracked for 48 h with 24 h exposure to ATZ followed by 24 h relaxation in ATZ-free culture medium as shown in Fig. 4A. Imaging was performed towards the end of 24 and 48 h as shown in Fig. 4A with representative images of transfected cells shown in Fig. 4B and C, respectively. Consistent with our previous findings, cells treated with ATZ for 24 h exhibit decreased fluorescence intensity, suggesting a lowering in global ^{me}CpG levels. The relative decrease of intensity is ~15% and ~27% for 3 and 30 ppb treatment groups respectively as shown Fig. 4D. After relaxation, changes in ^{me}CpG seem to amplify. A decrease of ~31 and ~49% in ^{me}CpG was observed for cells treated with 3 and 30 ppb ATZ, respectively.

Histogram reveals the intrinsic heterogeneity in ^{me}CpG of HEK293T cells with and without treatments as shown in Fig. 4E and **F**. Untreated cells exhibit similar looking histogram at 24 and 48 h of assessment. After treating with ATZ, the histogram exhibits a rightward shifting suggesting decreased levels of ^{me}CpG both at 24 and 48 h observation point. The reduction is more significant after relaxation than prior to, suggesting that the alterations in ^{me}CpG tend to persist and even amplify after the removal of ATZ. The observed changes are similar between two tested doses, namely 3 and 30 ppb.

4. Discussion

ATZ is an environmental chemical commonly found in soil and water. Currently, the maximum contaminant level (MCL) of ATZ in water is set to be 3 ppb by the U.S. EPA (Rohr and McCoy, 2009; EPA, 2016). ATZ concentrations exceeding the regulation limit have been reported in drinking water supplies in several regions in the U.S. (Strosnider et al., 2017; Almberg et al., 2018) For instance, ATZ concentrations of ~6 ppb were found in community water systems in rural Indiana, U.S. (Ochoa-Acuña et al., 2009) Studies from various animals have shown that ATZ concentrations up to 30 ppb can alter the transcriptome while minimal mortality and morphological changes were observed (Wirbisky et al., 2015; Wirbisky-Hershberger et al., 2017). We thus selected to work with 3 and 30 ppb ATZ to explore its low-dose toxicity and potentially long-term health implications using a model cell line HEK293T. HEK293T cells were selected as a model system, since extensive evidence exists suggesting that ATZ gets enriched and degraded in human kidneys (Catenacci et al., 2002; Perry et al., 2000Perry et al., 2000), thus making it an organ susceptible for ATZ induced damages. HEK293T cells exposed to a low dose of ATZ ($\leq$30 ppb) did not induce changes in either metabolic activities, cell growth rates, or morphologies. ATZ at the selected doses did not elicit any mutagenic activities. These findings are consistent with literature reports suggesting that ATZ lower than 30 ppb does not significantly alter the morphology or phenotypic behavior of animals immediately after exposure (Filipov et al., 2005; Du Preez et al., 2008).

H3K9me3 is the hallmark of permanently suppressed heterochromatin, also known as constitutive heterochromatin (Bannister and Kouzarides, 2011). During development, constitutive heterochromatin is typically established towards the end of differentiation and is thus considered as a potential hallmark for terminally differentiated cells(Becker et al., 2016). Aberrant alterations in H3K9me3 is typically observed in cancer cells and neurodegenerative diseases like Huntington's and Parkinson's Disease (Yokoyama et al., 2013; Berson et al., 2018; Cobos et al., 2019). Our results suggest that exposure to ATZ significantly lowers the global H3K9me3 levels, by ~14% and ~29% for ATZ concentrations of 3 and 30 ppb, respectively. To the best of our knowledge, there are no previous studies examining ATZ effects on H3K9me3 levels and distributions. The reduction in global H3K9me3 levels suggest the potential disappearance of well-defined heterochromatin regions which can be indicative of increased cellular plasticity (Bošković et al., 2014; Becker et al., 2016). Specifically, the well-defined H3K9me3 foci at nuclear periphery almost completely disappeared after treating with high doses of ATZ while the number of H3K9me3 foci is found not significantly altered after ATZ treatments as shown in Fig. S6B, which collectively suggest that the loss of H3K9me3 occurs with a spatial preference. Previous work has shown that bisphenol A (BPA), a recognized EDC, can reduce H3K9me3 levels in human SH-SY5Y cells after treating with 10 μM BPA for 96 h (Senyildiz et al., 2017). Similar observations have been made in mouse oocytes exposure experiments (Trapphoff et al., 2013). Polychlorinated biphenyl (PCB) 77 or 126 are another type of EDC with known impact on epigenome. Previous studies have shown that human endothelial cells show decreased H3K9me3 levels in selected gene loci, e.g., p65, an inflammatory associated gene (Liu et al., 2015). Our observation here thus aligns with the known epigenetic effects of EDC. The observed changes arising from exposure to ATZ, however, cannot be explained by alterations in the expression levels of epigenetic enzymes, since their

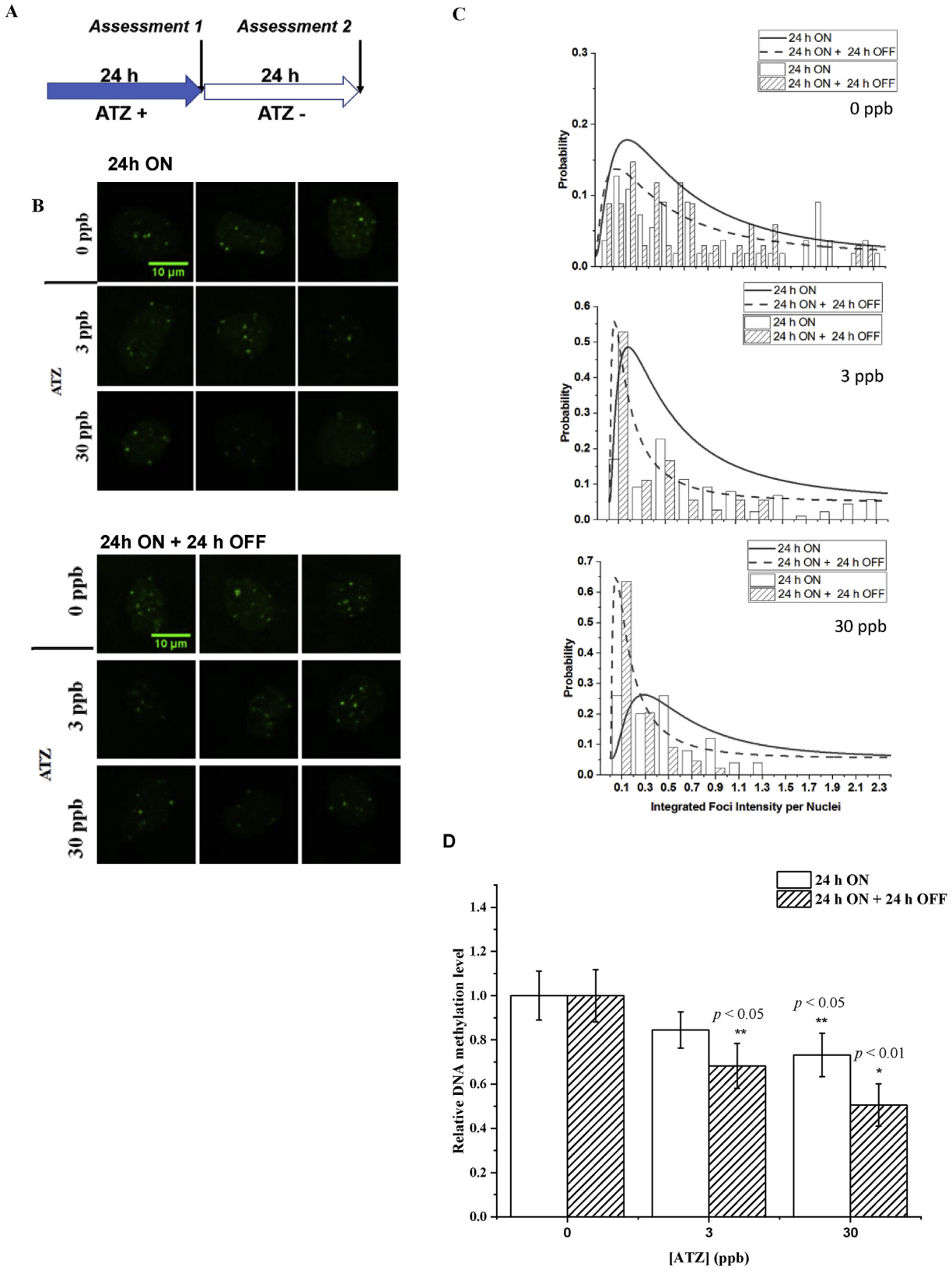

Fig. 4. Reduction in DNA methylation levels in HEK293T cells exposed to ATZ persist after a relaxation period. A. Schematic time course of HEK293T cells exposure to ATZ and relaxation cycle. Assessment 1 or exposure period (24 h ON) and assessment 2 or relaxation period (24 h ON + 24 h OFF). **B.** Representative cell images of HEK2937T cells during assessments 1 and 2 at different ATZ concentrations, 0, 3 and 30 ppb. **C.** Probability density distributions of the integrated intensity per nuclei obtained from single cell image analysis for assessments 1 and 2**. D.** Relative DNA methylation level obtained for assessments 1 and 2.

expression levels were found not significantly altered by ATZ.

^{me}CpG accounts for methylation in CpG sites that are most frequently found in eukaryotic cells. ^{me}CpG is most abundant in promoter regions of repressed genes and is also found in the exons of actively transcribed genes. Compared to other histone-based epigenetic modifications, ^{me}CpG patterns are well preserved during cell divisions and thus can be passed to the next generation. Alterations in ^{me}CpG patterns have been postulated to be persistent and work as a cellular memory of past environmental exposure histories. We thus evaluated the impact of exposure to ATZ on the methylation pattern of HEK293T cells and found a drop of 23 and 32% in ^{me}CpG for cells exposed to ATZ of 3 and 30 ppb, respectively. Our results suggest that exposure to ATZ can lead to significant reductions in ^{me}CpG levels manifested primarily as the loss of dense CpG islands within cell nucleus and particularly near the periphery. There is no previous study assessing ATZ effects on ^{me}CpG using a human cell line to the best of our knowledge. The general findings, however, is consistent with what has been reported using various animal models. Specifically, studies using juvenile common carp find that ^{me}CpG is significantly reduced in various tissues including liver, kidney, gill, gonad, and brain after exposure to ATZ (Wang et al., 2014; Xing et al., 2015). The reduction ranges from 10 to 45% depending on the type of tissues with a ATZ dose ranging between 4.28 and 428 μg/L (ppb) (Wang et al., 2014; Xing et al., 2015). Similarly, exposed Japanese medaka (*Oryzias latipes*) to 5 or 50 μg/L of ATZ showed a reduction in global DNA methylation in testis and ovaries of 1.27- and 1.85-fold relative to control, respectively (Cleary et al., 2019). In our previous study using a zebrafish model, we also observed 36 and 56% reductions in ^{me}CpGs when embryos were exposed to 3 ppb and 30 ppb of ATZ for 72 h post-fertilization, respectively (Wirbisky-Hershberger et al., 2017). Human cells exposed to another recognized EDC, namely BPA, have shown a reduction of 36% in ^{me}CpG after 96 h of exposure (Karaman et al., 2019). The percentage of reductions that we observed in HEK293T are essentially in the same ballpark. The observed reduction in ^{me}CpG can be partially attributed to the altered transcriptional levels of DNMT and TET but may also has contributions from altered DNMT activities resulting from exposure to ATZ. Our previous study has shown that DNMT1 can have ~13 and 38% reductions in their activity after exposure to 3 and 30 ppb ATZ, respectively (Wirbisky-Hershberger et al., 2017). We thus expect that cells will gradually lose ^{me}CpG patterns after each cell division.

Interestingly, the observed changes in ^{me}CpG are similar to what we have discovered for H3K9me3. This trend can be potentially interpreted via a strong correlation/cross-talking between DNA methylation and H3K9me3 in eukaryotic cells. Previous literature evidence has shown that loss of ^{me}CpG can alter H3K9me3 pattern particularly in heterochromatin regions (Tariq et al., 2003). Changes in SUV39H methyltransferase activity, a histone methyltransferase responsible for methylating H3K9 during mitosis, can lead to equivalent alterations in DNA methylation levels (Lehnertz et al., 2003). Furthermore, direct molecular interactions have been reported between SUV39H and DNMT1 and DNMT3A/B (Fuks et al., 2003; Rose and Klose, 2014). The changes observed in H3K9me3, are thus likely to arise from the reduced presence of DNMT1 during mitosis which are essential for recruiting SUV39H to ensure the inheritance of H3K9me3 patterns in the next progeny which subsequently result in the loss of H3K9me3 in cell populations.

Epigenetic changes are potentially reversible due to the presence of epigenetic writer and eraser enzymes. Our finding suggests that ATZ-induced alterations in ^{me}CpG can persist and amplify after the removal of exposure source leading to possible long-term health concerns. Long-term effects of chronic exposure to ATZ has been studied. In a previous zebrafish study, 72 h of exposure to ATZ during embryogenesis can induce damages that persist throughout maturation and lead to dysregulations in hormonal release of adult zebra fish (Wirbisky et al., 2015). This sustained damage can be a potential consequence of ATZ induced persistent epigenome alterations, which has been reported by a previous study using common carp. In this study, 40 days of exposure to ATZ in juvenile fish causes DNA hypomethylation in the kidneys, and the decreased methylation levels persisted after the 40 days recovery period (Wang et al., 2014). To the best of our knowledge, however, no similar ATZ studies have been performed on mammalian cell models. Similar to zebra- and carp fish studies, our results in mammalian cells suggest the altered DNA methylation profile does not immediately recover from the withdraw of ATZ. Furthermore, the effect can potentially persist through cell division. The persistency of altered DNA methylation level was consistent with previous studies that assessing the dynamic features of acquired epigenetic modifications Sánchez et al., 2019(Bintu et al., 2016). Taking together, our studies provide new insights into the ATZ induced ^{me}CpG dysregulation in mammals.

5. Conclusions

Exposure to ATZ can cause deterioration of multiple organs in animals. The underlying molecular mechanism conferring long-term adverse health outcomes, however, remain elusive. Here we assessed the effects of ATZ on selected epigenetic marks, namely ^{me}CpG and H3K9me3. Using HEK293T as a human cell line model we found that exposure to ATZ significantly downregulates ^{me}CpG and H3K9me3, while minimal perturbations were observed in cellular metabolic, morphological and proliferative properties. The observed changes in ^{me}CpG can be at least partially explained by the alterations in the expression patterns of epigenetic enzymes regulating DNA methylation. H3K9me3 exhibits a similar trend of changes arising potentially from the cross-talking of DNA and histone methylation. Changes in ^{me}CpG were found to be a better clustering feature distinguishing between treated and untreated cells and thus were evaluated for its persistency. 24 h after removal of ATZ, we found that ^{me}CpG changes persist suggesting a plausible long-term effect.

Acknowledgments

This work was supported by the U.S. Army Medical Research (Award Number: W81XWH-14-1-0012), National Science Foundation [CBET-1512285 & CBET-1705560], and the Administrative Department of Science, Technology and Innovation (COLCIENCIAS) from Colombia and Fulbright (Grant 529) (O.F.S.). The authors declare no conflict of interest.

Appendix A. Supplementary data

Supplementary data to this article can be found online at https://doi.org/10.1016/j.envpol.2019.113712.

References

Alavian-Ghavanini, A., Rüegg, J., 2018. Understanding epigenetic effects of endocrine disrupting chemicals: from mechanisms to novel test methods. Basic Clin. Pharmacol. Toxicol. 122, 38–45.

Almberg, K., Turyk, M., Jones, R., Rankin, K., Freels, S., Stayner, L., 2018. Atrazine contamination of drinking water and adverse birth outcomes in community water systems with elevated atrazine in Ohio, 2006–2008. Int. J. Environ. Res. Public Health 15, 1889.

Bannister, A.J., Kouzarides, T., 2011. Regulation of chromatin by histone modifications. Cell Res. 21, 381.

Barreto, G., Schäfer, A., Marhold, J., Stach, D., Swaminathan, S.K., Handa, V., Döderlein, G., Maltry, N., Wu, W., Lyko, F., 2007. Gadd45a promotes epigenetic gene activation by repair-mediated DNA demethylation. Nature 445, 671.

Becker, J.S., Nicetto, D., Zaret, K.S., 2016. H3K9me3-Dependent heterochromatin:

barrier to cell fate changes. Trends Genet. : TIG (Trends Genet.) 32, 29–41.
Berson, A., Nativio, R., Berger, S.L., Bonini, N.M., 2018. Epigenetic regulation in neurodegenerative diseases. Trends Neurosci. 41, 587–598.
Bintu, L., Yong, J., Antebi, Y.E., McCue, K., Kazuki, Y., Uno, N., Oshimura, M., Elowitz, M.B., 2016. Dynamics of epigenetic regulation at the single-cell level. Science 351, 720–724.
Bird, A., 2002. DNA methylation patterns and epigenetic memory. Genes Dev. 16, 6–21.
Bošković, A., Eid, A., Pontabry, J., Ishiuchi, T., Spiegelhalter, C., Raghu Ram, E.V.S., Meshorer, E., Torres-Padilla, M.-E., 2014. Higher chromatin mobility supports totipotency and precedes pluripotency in vivo. Genes Dev. 28, 1042–1047.
Bustin, S.A., Benes, V., Garson, J.A., Hellemans, J., Huggett, J., Kubista, M., Mueller, R., Nolan, T., Pfaffl, M.W., Shipley, G.L., Vandesompele, J., Wittwer, C.T., 2009. The MIQE guidelines: minimum information for publication of quantitative real-time PCR experiments. Clin. Chem. 55, 611–622.
Capoulade, J., Wachsmuth, M., Hufnagel, L., Knop, M., 2011. Quantitative fluorescence imaging of protein diffusion and interaction in living cells. Nat. Biotechnol. 29, 835.
Carpenter, A.E., Jones, T.R., Lamprecht, M.R., Clarke, C., Kang, I.H., Friman, O., Guertin, D.A., Chang, J.H., Lindquist, R.A., Moffat, J., Golland, P., Sabatini, D.M., 2006. CellProfiler: image analysis software for identifying and quantifying cell phenotypes. Genome Biol. 7, R100.
Catenacci, G., Colli, G., Verni, P., Barisano, A., 2002. Environmental and biological monitoring of occupational exposure in atrazine formulating plant. Giornale italiano di medicina del lavoro ed ergonomia 24, 35–42.
Cleary, J.A., Tillitt, D.E., vom Saal, F.S., Nicks, D.K., Claunch, R.A., Bhandari, R.K., 2019. Atrazine induced transgenerational reproductive effects in medaka (Oryzias latipes). Environ. Pollut. 251, 639–650.
Cobos, S.N., Bennett, S.A., Torrente, M.P., 2019. The impact of histone post-translational modifications in neurodegenerative diseases. Biochim. Biophys. Acta (BBA) - Mol. Basis Dis. 1865, 1982–1991.
Diamanti-Kandarakis, E., Bourguignon, J.-P., Giudice, L.C., Hauser, R., Prins, G.S., Soto, A.M., Zoeller, R.T., Gore, A.C., 2009. Endocrine-disrupting chemicals: an endocrine society scientific statement. Endocr. Rev. 30, 293–342.
Du Preez, L.H., Kunene, N., Everson, G.J., Carr, J.A., Giesy, J.P., Gross, T.S., Hosmer, A.J., Kendall, R.J., Smith, E.E., Solomon, K.R., 2008. Reproduction, larval growth, and reproductive development in African clawed frogs (Xenopus laevis) exposed to atrazine. Chemosphere 71, 546–552.
EPA, U., 2016. Refined Ecological Risk Assessment for Atrazine. Office of Pesticide Programs, Washington, DC.
Filipov, N.M., Pinchuk, L.M., Boyd, B.L., Crittenden, P.L., 2005. Immunotoxic effects of short-term atrazine exposure in young male C57BL/6 mice. Toxicol. Sci. 86, 324–332.
Fischle, W., Franz, H., Jacobs, S.A., Allis, C.D., Khorasanizadeh, S., 2008. Specificity of the chromodomain Y chromosome family of chromodomains for lysine-methylated ARK (S/T) motifs. J. Biol. Chem. 283, 19626–19635.
Flatau, E., Gonzales, F., Michalowsky, L., Jones, P., 1984. DNA methylation in 5-aza-2'-deoxycytidine-resistant variants of C3H 10T1/2 C18 cells. Mol. Cell. Biol. 4, 2098–2102.
Fuks, F., Hurd, P.J., Deplus, R., Kouzarides, T., 2003. The DNA methyltransferases associate with HP1 and the SUV39H1 histone methyltransferase. Nucleic Acids Res. 31, 2305–2312.
Gonzalez-Sandoval, A., Towbin, B.D., Kalck, V., Cabianca, D.S., Gaidatzis, D., Hauer, M.H., Geng, L., Wang, L., Yang, T., Wang, X., 2015. Perinuclear anchoring of H3K9-methylated chromatin stabilizes induced cell fate in C. elegans embryos. Cell 163, 1333–1347.
Graymore, M., Stagnitti, F., Allinson, G., 2001. Impacts of atrazine in aquatic ecosystems. Environ. Int. 26, 483–495.
Hanson, M.A., Skinner, M.K., 2016. Developmental origins of epigenetic transgenerational inheritance. Environ. Epigenet. 2, dvw002.
Hao, C., Gely-Pernot, A., Kervarrec, C., Boudjema, M., Becker, E., Khil, P., Tevosian, S., Jégou, B., Smagulova, F., 2016. Exposure to the widely used herbicide atrazine results in deregulation of global tissue-specific RNA transcription in the third generation and is associated with a global decrease of histone trimethylation in mice. Nucleic Acids Res., gkw840
Hayashi-Takanaka, Y., Yamagata, K., Wakayama, T., Stasevich, T.J., Kainuma, T., Tsurimoto, T., Tachibana, M., Shinkai, Y., Kurumizaka, H., Nozaki, N., 2011. Tracking epigenetic histone modifications in single cells using Fab-based live endogenous modification labeling. Nucleic Acids Res. 39, 6475–6488.
Hyun, K., Jeon, J., Park, K., Kim, J., 2017. Writing, erasing and reading histone lysine methylations. Exp. Mol. Med. 49, e324.
Jørgensen, H.F., Adie, K., Chaubert, P., Bird, A.P., 2006. Engineering a high-affinity methyl-CpG-binding protein. Nucleic Acids Res. 34 e96-e96.
Karaman, E.F., Caglayan, M., Sancar-Bas, S., Ozal-Coskun, C., Arda-Pirincci, P., Ozden, S., 2019. Global and region-specific post-transcriptional and post-translational modifications of bisphenol A in human prostate cancer cells. Environ. Pollut. 255, 113318.
Kiely, T., Donaldson, D., Grube, A., 2004. Pesticide Industry Sales and Usage: 2000 and 2001 Market Estimates. US Environmental Protection Agency, Washington, DC.
Kim, S.-E., Chang, M., Yuan, C., 2014. One-pot approach for examining the DNA methylation patterns using an engineered methyl-probe. Biosens. Bioelectron. 58, 333–337.
Lebov, J., Engel, L., Richardson, D., Hogan, S., Hoppin, J., Sandler, D., 2016. Pesticide use and risk of end-stage renal disease among licensed pesticide applicators in the Agricultural Health Study. Occup. Environ. Med. 73 (1), 3–12.
Lehnertz, B., Ueda, Y., Derijck, A.A., Braunschweig, U., Perez-Burgos, L., Kubicek, S., Chen, T., Li, E., Jenuwein, T., Peters, A.H., 2003. Suv39h-mediated histone H3 lysine 9 methylation directs DNA methylation to major satellite repeats at pericentric heterochromatin. Curr. Biol. 13, 1192–1200.
Liu, D., Perkins, J.T., Petriello, M.C., Hennig, B., 2015. Exposure to coplanar PCBs induces endothelial cell inflammation through epigenetic regulation of NF-κB subunit p65. Toxicol. Appl. Pharmacol. 289, 457–465.
Liu, W., Du, Y., Liu, J., Wang, H., Sun, D., Liang, D., Zhao, L., Shang, J., 2014. Effects of atrazine on the oxidative damage of kidney in Wister rats. Int. J. Clin. Exp. Med. 7, 3235–3243.
Lungu, C., Pinter, S., Broche, J., Rathert, P., Jeltsch, A., 2017. Modular fluorescence complementation sensors for live cell detection of epigenetic signals at endogenous genomic sites. Nat. Commun. 8, 649.
Mark, M.v.d., Brouwer, M., Kromhout, H., Nijssen, P., Huss, A., Vermeulen, R., 2012. Is pesticide use related to Parkinson disease? Some clues to heterogeneity in study results. Environ. Health Perspect. 120, 340–347.
Mostafalou, S., Abdollahi, M., 2013. Pesticides and human chronic diseases: evidences, mechanisms, and perspectives. Toxicol. Appl. Pharmacol. 268, 157–177.
Mostafalou, S., Abdollahi, M., 2017. Pesticides: an update of human exposure and toxicity. Arch. Toxicol. 91, 549–599.
Nightingale, K.P., Gendreizig, S., White, D.A., Bradbury, C., Hollfelder, F., Turner, B.M., 2007. Cross-talk between histone modifications in response to histone deacetylase inhibitors MLL4 links histone H3 acetylation and histone H3K4 methylation. J. Biol. Chem. 282, 4408–4416.
Ochoa-Acuña, H., Frankenberger, J., Hahn, L., Carbajo, C., 2009. Drinking-water herbicide exposure in Indiana and prevalence of small-for-gestational-age and preterm delivery. Environ. Health Perspect. 117, 1619.
Pathak, R., Dikshit, A., 2011. Atrazine and human health. Int. J. Ecosys. 1, 14–23.
Perry, M., Christiani, D., Dagenhart, D., Tortorelli, J., Singzoni, B., 2000. Urinary biomarkers of atrazine exposure among farm pesticide applicators. Ann. Epidemiol. 10 (7), 479.
Politz, J.C.R., Scalzo, D., Groudine, M., 2013. Something silent this way forms: the functional organization of the repressive nuclear compartment. Annu. Rev. Cell Dev. Biol. 29, 241–270.
Rohr, J.R., McCoy, K.A., 2009. A qualitative meta-analysis reveals consistent effects of atrazine on freshwater fish and amphibians. Environ. Health Perspect. 118, 20–32.
Rose, N.R., Klose, R.J., 2014. Understanding the relationship between DNA methylation and histone lysine methylation. Biochimica et Biophysica Acta (BBA) - Gene Regulatory Mechanisms 1839, 1362–1372.
Sanchez, O.F., Mendonca, A., Carneiro, A.D., Yuan, C., 2017. Engineering recombinant protein sensors for quantifying histone acetylation. ACS Sens. 2, 426–435.
Sánchez, O.F., Mendonca, A., Min, A., Liu, J., Yuan, C., 2019. Monitoring histone methylation (H3K9me3) changes in live cells. ACS Omega 4 (8), 13250–13259.
Sanchez, O.F., Williamson, D., Cai, L., Yuan, C., 2015. A sensitive protein-based sensor for quantifying histone acetylation levels. Talanta 140, 212–218.
Schug, T.T., Janesick, A., Blumberg, B., Heindel, J.J., 2011. Endocrine disrupting chemicals and disease susceptibility. J. Steroid Biochem. Mol. Biol. 127, 204–215.
Sena, L.R., 2017. Hepatotoxic and Nephrotoxic Effects of Atrazine on Adult Male xenopus Laevis Frogs: a Laboratory Study.
Senyildiz, M., Karaman, E.F., Bas, S.S., Pirincci, P.A., Ozden, S., 2017. Effects of BPA on global DNA methylation and global histone 3 lysine modifications in SH-SY5Y cells: an epigenetic mechanism linking the regulation of chromatin modifying genes. Toxicol. In Vitro 44, 313–321.
Skinner, M.K., Manikkam, M., Guerrero-Bosagna, C., 2010. Epigenetic transgenerational actions of environmental factors in disease etiology. Trends Endocrinol. Metab. 21, 214–222.
Strosnider, H., Kennedy, C., Monti, M., Yip, F., 2017. Rural and urban differences in air quality, 2008–2012, and community drinking water quality, 2010–2015—United States. MMWR Surveillance Summ. 66, 1.
Sun, Y., Li, Y.-S., Li, B., Ma, K., Li, B.-X., 2017. A study of the age-related effects of lactational atrazine exposure. Reprod. Toxicol. 69, 230–241.
Tapia-Orozco, N., Santiago-Toledo, G., Barron, V., Espinosa-García, A.M., García-García, J.A., Garcia-Arrazola, R., 2017. Environmental epigenomics: current approaches to assess epigenetic effects of endocrine disrupting compounds (EDC's) on human health. Environ. Toxicol. Pharmacol. 51, 94–99.
Tariq, M., Saze, H., Probst, A.V., Lichota, J., Habu, Y., Paszkowski, J., 2003. Erasure of CpG methylation in Arabidopsis alters patterns of histone H3 methylation in heterochromatin. Proc. Natl. Acad. Sci. 100, 8823–8827.
Thelin, G.P., Stone, W.W., 2010. Method for Estimating Annual Atrazine Use for Counties in the Conterminous United States, 1992-2007. US Department of the Interior, US Geological Survey.
Trapphoff, T., Heiligentag, M., El Hajj, N., Haaf, T., Eichenlaub-Ritter, U., 2013. Chronic exposure to a low concentration of bisphenol A during follicle culture affects the epigenetic status of germinal vesicles and metaphase II oocytes. Fertil. Steril. 100, 1758-1767.e1751.
Uzumcu, M., Zama, A.M., Oruc, E., 2012. Epigenetic mechanisms in the actions of endocrine-disrupting chemicals: gonadal effects and role in female reproduction. Reprod. Domest. Anim. 47, 338–347.
Wang, C., Zhang, Z., Yao, H., Zhao, F., Wang, L., Wang, X., Xing, H., Xu, S., 2014. Effects of atrazine and chlorpyrifos on DNA methylation in the liver, kidney and gill of the common carp (Cyprinus carpio L.). Ecotoxicol. Environ. Saf. 108, 142–151.
Wang, X., Xing, H., Jiang, Y., Wu, H., Sun, G., Xu, Q., Xu, S., 2013. Accumulation, histopathological effects and response of biochemical markers in the spleens

and head kidneys of common carp exposed to atrazine and chlorpyrifos. Food Chem. Toxicol. 62, 148–158.
Wei, F., Huang, J., Li, H., 2011. Variable selection and estimation in high-dimensional varying-coefficient models. Stat. Sin. 21, 1515–1540.
Wirbisky-Hershberger, S.E., Sanchez, O.F., Horzmann, K.A., Thanki, D., Yuan, C., Freeman, J.L., 2017. Atrazine exposure decreases the activity of DNMTs, global DNA methylation levels, and dnmt expression. Food Chem. Toxicol. 109, 727–734.
Wirbisky, S.E., Freeman, J.L., 2015. Atrazine exposure and reproductive dysfunction through the hypothalamus-pituitary-gonadal (HPG) Axis. Toxics 3, 414–450.
Wirbisky, S.E., Weber, G.J., Sepúlveda, M.S., Xiao, C., Cannon, J.R., Freeman, J.L., 2015. Developmental origins of neurotransmitter and transcriptome alterations in adult female zebrafish exposed to atrazine during embryogenesis. Toxicology 333, 156–167.
Xin, F., Susiarjo, M., Bartolomei, M.S., 2015. Multigenerational and transgenerational effects of endocrine disrupting chemicals: a role for altered epigenetic regulation? Semin. Cell Dev. Biol. 43, 66–75.
Xing, H., Li, S., Wang, Z., Gao, X., Xu, S., Wang, X., 2012. Histopathological changes and antioxidant response in brain and kidney of common carp exposed to atrazine and chlorpyrifos. Chemosphere 88, 377–383.
Xing, H., Wang, C., Wu, H., Chen, D., Li, S., Xu, S., 2015. Effects of atrazine and chlorpyrifos on DNA methylation in the brain and gonad of the common carp. Comp. Biochem. Physiol. C Toxicol. Pharmacol. 168, 11–19.
Yokoyama, Y., Hieda, M., Nishioka, Y., Matsumoto, A., Higashi, S., Kimura, H., Yamamoto, H., Mori, M., Matsuura, S., Matsuura, N., 2013. Cancer-associated upregulation of histone H3 lysine 9 trimethylation promotes cell motility in vitro and drives tumor formation in vivo. Cancer Sci. 104, 889–895.